

# Anomalous Diffusion and Superdiffusion in Integrable Spin Chains via a Hard-Rod Gas Mapping

Andrew Urilyon <sup>1,2</sup> Romain Vasseur <sup>3</sup> Sarang Gopalakrishnan <sup>4</sup> and Jacopo De Nardis <sup>1,2</sup>

<sup>1</sup>Laboratoire de Physique Théorique et Modélisation, CNRS UMR 8089, CY Cergy Paris Université, 95302 Cergy-Pontoise Cedex, France

<sup>2</sup>JEIP, UAR 3573 CNRS, Collège de France, PSL Research University, 11 Place Marcelin Berthelot, 75321 Paris Cedex 05, France

<sup>3</sup>Department of Theoretical Physics, University of Geneva, 24 quai Ernest-Ansermet, 1211 Geneva, Switzerland

<sup>4</sup>Department of Electrical and Computer Engineering, Princeton University, Princeton, NJ 08544, USA

We introduce a multi-species generalization of the hard-rod gas in which each species has a distinct effective length, and the repulsive scattering shift is set by the smaller of the two colliding rods. We argue that this model shares key quasiparticle and scattering features with the XXZ spin chain. We show that fixing only the functional decay of bare velocities with rod length is sufficient to reproduce the XXZ spin-transport phase diagram: diffusion (with anomalous fluctuations) in the anisotropic regime and superdiffusion at the isotropic point. We then demonstrate that the statistics of *charge transfer* differs qualitatively from that of *particle trajectories*. For long rods, trajectories are Gaussian in the diffusive regime and appear to exhibit KPZ statistics at the isotropic point, providing a direct microscopic signature of KPZ physics in integrable quasiparticle motion. In contrast, charge-transfer fluctuations are anomalous in the anisotropic regime, while they cross over to Gaussian statistics at late times at the isotropic point, reconciling non-Gaussian trajectory fluctuations with Gaussian charge-transfer statistics. Our results establish classical hard-rod dynamics as a minimal yet quantitatively faithful framework for anomalous spin and charge transport in integrable systems, and offer new insight into the origin of KPZ fluctuations in isotropic integrable models.

**Introduction.** Strongly interacting many-body systems are notoriously difficult to describe, yet they can exhibit behavior that is qualitatively distinct from the familiar weak-coupling or dilute limits, especially out of equilibrium. A central arena where nonequilibrium physics has historically revealed such qualitative differences is transport theory. While the transport of particles and charges is often *normal*, that is, diffusive, robust and sometimes universal exceptions are known to arise in low-dimensional systems.

A prominent example is the anomalous transport of spin or charge in one-dimensional quantum systems, which has received considerable attention in recent years [1–42]. Although integrable systems are typically expected to display ballistic transport [43–51], and non-integrable systems with momentum conservation often exhibit anomalous hydrodynamic tails consistent with Kardar–Parisi–Zhang (KPZ) or Lévy-type universality classes [52–55], it came as a surprise that *isotropic* integrable spin chains can themselves exhibit KPZ fluctuations [56–71], an unexpected phenomenon that has also been recently confirmed experimentally [72–74].

Despite the intense activity it has generated, a fully established microscopic explanation for the emergence of KPZ scaling in these settings is still missing: current understanding relies largely on scaling arguments that fix the dynamical exponent [58] and on partial formulations of nonlinear fluctuating hydrodynamic theory [62, 75]. Moreover, integrable models can display a distinct form of anomalous transport in the guise of

diffusion with anomalous fluctuations [76–83]. In the XXZ spin chain away from the isotropic case, this can be traced to the interplay between ballistically propagating magnons and their bound states: the effective spin carried by fast quasiparticles is dynamically screened through interactions with large bound states [84], while

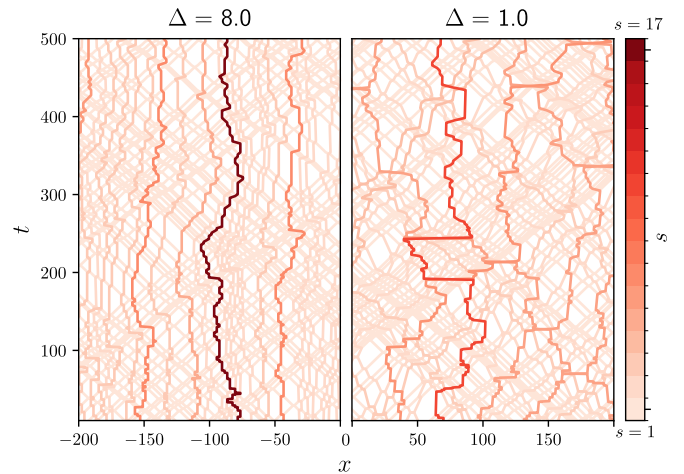


Figure 1. Particle trajectories for  $\Delta = 8$  and  $\Delta = 1$  for different sizes  $s$ . Due to the distinct bare-velocity behavior, the motion of large particles in the  $\Delta = 8$  case is dominated by collisions with small particles with  $s = 1$ , resulting in random-walk-like behavior. In the case of  $\Delta = 1$ , large particles of size  $s$  experience jumps  $O(s)$  caused by scattering with other large ones, leading to non-linear, long-time tails.

scattering-induced shifts and the randomization of quasiparticle ballistic trajectories in generic thermodynamic stationary states generate anomalous diffusive fluctuations. How such anomalous fluctuations conspire at the isotropic point to give KPZ-like fluctuations remains a mystery.

**Summary of results.** We introduce and analyze a minimal *classical* toy model for XXZ quasiparticle dynamics: a one-dimensional multi-species hard-rod gas [85–95] in which species represent bound states (“strings”) of different lengths, each carrying two velocities (right/left movers) and interacting through collisions that implement a prescribed scattering shift; see Eqs. (2) and (4). Despite its minimal ingredients, the model reproduces and clarifies key features of spin transport in the Heisenberg chain. At the isotropic point, large particles undergo rare, large displacements due to collisions with other large species (Fig. 1), producing a crossover from KPZ to normal fluctuations of *trajectories* (Fig. 2) and yielding superdiffusive *charge* transport with asymptotically Gaussian charge fluctuations (Fig. 4), consistent with experiments [74] and numerics [80, 96, 97]. Away from isotropy, we recover a single-file diffusion picture: large particles are effectively immobilized and move mainly through collisions with ballistically propagating light particles (Fig. 1). Notably, all quasiparticles carry positive charge: screening and anomalous diffusion arise not from cancellations between opposite carriers, but from *strong dynamical correlations* across species (Eq. (14) and Fig. 3). Overall, this provides a first study of Heisenberg-chain quasiparticle dynamics via a classical hard-rod model, demonstrating the microscopic emergence of anomalous diffusion and superdiffusion, and giving direct access to *single-quasiparticle trajectories*.

**The multi-species hard-rod gas.** The spin- $\frac{1}{2}$  XXZ chain is defined by

$$H = \sum_j \left( S_j^x S_{j+1}^x + S_j^y S_{j+1}^y + \Delta S_j^z S_{j+1}^z \right). \quad (1)$$

It is Bethe-ansatz solvable [98–101]: its thermodynamic spectrum consists of magnons and bound states (strings) labeled by an integer size  $s \geq 1$  and rapidity  $\theta$ . For  $|\Delta| \geq 1$  there is no upper bound on  $s$ , and thermal states populate large particles. The key distinction between the isotropic point ( $\Delta = 1$ ) and the gapped anisotropic regime ( $\Delta > 1$ ) is the scaling of effective velocities: algebraic in  $s$  at  $\Delta = 1$  (semi-classical large- $s$  excitations [102, 103]) and exponential in  $s$  for  $\Delta > 1$ . To isolate the minimal ingredient behind the transport phenomenology, we introduce a classical integrable proxy: a multi-species hard-rod gas whose only essential input is this  $s$ -dependence of velocities. We consider species  $s = 1, \dots, s_{\max}$  with two chiralities  $\sigma = \pm 1$ , bare velocities (with  $\eta = \text{arccosh}(\Delta)$ )  $v_s^\sigma = \sigma e^{-(s-1)\eta}/s^2$  and equilibrium densities  $\bar{\rho}_s = 1/(s(s+1)(s+2))$ , chosen to satisfy half filling  $\sum_{s \geq 1} s \bar{\rho}_s = 1/2$ . The parameter  $\eta \geq 0$

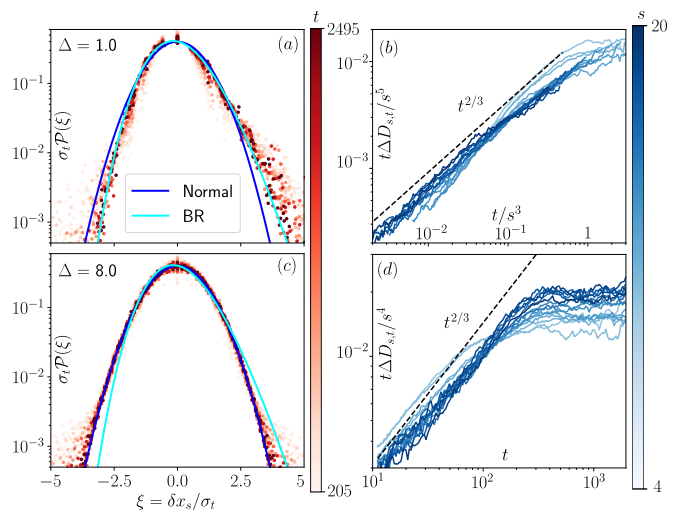


Figure 2. Plot of the distribution of fluctuations  $\mathcal{P}(\delta x_s)$  in Eq. (5) for right-moving particles  $\sigma = 1$  (also averaged with the left-movers with  $\xi \rightarrow -\xi$ ) and type  $s = 15 - 30$  for  $\Delta = 1$  and  $s = 5 - 10$  for  $\Delta = 8$ . The distribution is compared to a normalized Gaussian distribution and to a skewed KPZ distributions (Baik–Rains). All distributions are rescaled to have unit variance and zero mean. The right panel compares the approach to the asymptotic diffusion  $t\Delta_{s,t} = t(D_s(t) - D_s)$  (see Eq. (7)) rescaled with particle type and plotted against rescaled time  $t/s^3$  and unscaled time  $t$  for the  $\Delta = 1$  and  $\Delta = 8$  cases, respectively (see also Fig. 7 and 9).

interpolates between algebraic decay ( $\eta = 0$ ) and exponential suppression ( $\eta > 0$ ).

A (single-species) hard-rod gas is characterized by a constant two-body scattering shift equal to the rod length: quasiparticles preserve their bare velocities and interact through forward jumps at each collision. We generalize this structure to many species by prescribing the scattering length

$$\mathbf{a}_{s,s'} = 2 \min(s, s') - \delta_{s,s'}, \quad (2)$$

which mimics the “fusion” hierarchy of string interactions in the strongly anisotropic XXZ chain [104, 105]. The standard hard-rod gas is recovered by restricting to  $s_{\max} = 1$ , for which  $\mathbf{a}_{1,1} = 1$ . Although Eq. (2) is not the exact XXZ scattering phase shift at generic  $\Delta$ , we will show that it already captures the universal dynamical consequences of having many interacting species with a broad velocity distribution.

The physical intuition behind Eq. (2) can be phrased in terms of the notion of magnetization screening [58, 69, 84, 106–108]. In the large- $\Delta$  XXZ chain, domain-wall degrees of freedom are effectively conserved, and a small bound state traversing a larger one flips its internal orientation while crossing it; repeated encounters then randomize the sign carried by the small excitation, leading to an emergent cancellation of magnetization at long times. In our classical proxy, we implement the same screening

mechanism kinematically through the displacement field generated by the shifts in Eq. (2).

In this model all particles carry a positive “charge” proportional to their size, so the local magnetization density reads

$$m(x, t) = \lim_{s_{\max} \rightarrow \infty} \sum_{s=1}^{s_{\max}} s \rho_s(x, t) - 1/2, \quad (3)$$

where  $\rho_s(x, t)$  denotes the density of species  $s$  within an interval of size  $dx$  at position  $x$ . Despite the ballistic nature of the bare dynamics, interactions dress the trajectories in a highly nontrivial way. As in the usual hard-rod mapping, one may reduce the interacting dynamics to free point particles by shrinking rods to points and encoding interactions in cumulative shifts. Concretely, the trajectory  $x_{s,i}(t)$  (see Fig. 1) of the  $i$ -th particle of species  $s$  and chirality  $\sigma_i$  satisfies the implicit equation of motion

$$v_{s,i}^{\sigma_i} t + X_{s,i}^{(0)} = x_{s,i}(t) + \frac{1}{2} \sum_{s',j} \mathbf{a}_{s,s'} \text{sign}(x_{s,i}(t) - x_{s',j}(t)), \quad (4)$$

with  $X_{s,i}^{(0)}$  the initial position (chosen stochastically with classical Poissonian statistics and density fixed by  $\rho_s$ ). Equations of the form (4) can be obtained from a convex minimization principle (equivalently, an effective action), and provide an exact microscopic description of a strongly correlated integrable gas; see also [20, 109–112].

**Particle trajectories.** The microscopic dynamics generated by Eq. (4) is, in many respects, analogous to that of a standard hard-rod gas: quasiparticles retain their bare velocities, while interactions enter solely through cumulative position shifts produced by collisions. Upon coarse graining over many scattering events (in both time and space), one can characterize the large-scale motion of a tagged particle through its displacement

$$\delta x_{s,i}(t) = x_{s,i}(t) - x_{s,i}(0). \quad (5)$$

The corresponding effective velocity is defined as the long-time, ensemble-averaged drift. It can be computed using the same kinetic arguments as for the simple hard-rod gas [113], (see Fig. 8)

$$(v_s^\sigma)^{\text{eff}} = \lim_{t \rightarrow \infty} \frac{1}{t} \langle \delta x_{s,i}(t) \rangle = \sigma \frac{(s+2)e^{-\eta(s-1)}}{s(s+1)}, \quad (6)$$

where  $\langle \cdot \rangle$  denotes an average over the initial (thermal-stationary) configurations. Notice that this implies  $(v_s^\sigma)^{\text{eff}} \sim s^{-1}$  at the isotropic point, analogously to quasiparticle effective velocities in the XXX model.

Fluctuations around the mean drift define an effective *diffusion constant for particle trajectories*, which can be evaluated at a given time  $t$ ,

$$D_s(t) \equiv \frac{d}{dt} \left[ \langle (\delta x_{s,i}(t) - \langle \delta x_{s,i}(t) \rangle)^2 \rangle \right], \quad (7)$$

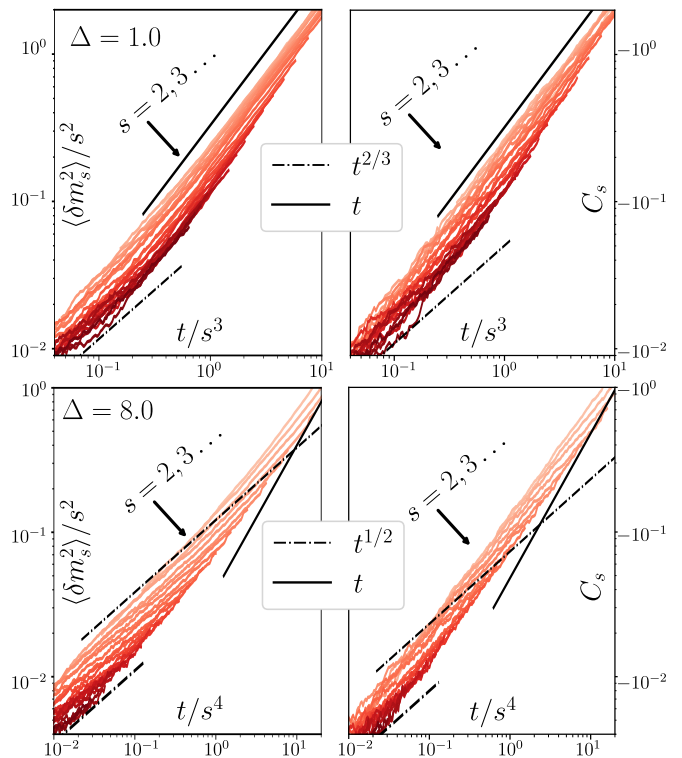


Figure 3. Behavior of the magnetization transfer for each species (see Eq. (11)),  $\langle \delta m_s^2 \rangle$  (left) and summed off-diagonal elements  $C_s = \sum_{s' \neq s} \langle \delta m_s \delta m_{s'} \rangle / s^2$  (right) for both  $\Delta = 1$  and  $\Delta = 8$ , demonstrating the presence of a transition from superdiffusive to ballistic behavior for  $\Delta = 1$  (top) and from diffusive to ballistic for  $\Delta > 1$  (bottom).

and whose infinite-time limit  $D_s = \lim_{t \rightarrow \infty} D_s(t)$  is *finite* for each fixed species  $s$ : in an interacting integrable gas, a tagged particle experiences an effectively random sequence of collisions at long times, which produces diffusive broadening of its trajectory. At first sight this seems paradoxical: *how can individual quasiparticle trajectories be diffusive, while the transported conserved charge displays superdiffusive spreading?* The resolution is that *large particles can build up anomalously large fluctuations before crossing over to normal diffusion at parametrically large time-scales*. The latter is directly related to the scaling of the diffusion constant with  $s$ . Indeed, in the anisotropic regime  $\Delta > 1$ , the diffusion constants  $D_s$  rapidly saturate to an  $s$ -independent value  $D_\infty$ , while at the isotropic point, one finds linear growth with  $s$ . An explicit evaluation yields (see End Matter for more details),

$$D_s = \frac{8}{9} \sum_{s'=1}^{\infty} \min \left( 1, \frac{(s+2)^3 s(s+1)}{(s'+2)^3 s'(s'+1)} \right) \left( \frac{s'+1}{s'} \right)^2 - \frac{2(1+4s)}{3s^2} \xrightarrow{s \rightarrow \infty} \frac{10}{9} s. \quad (8)$$

To then characterize particle trajectories, we introduce the scaling functions  $H_\Delta(z)$  with asymptotics given by

$H_\Delta(z \ll 1) \sim z^{-1/6}$  and  $H_\Delta(z \gg 1) = \text{const.}$  For  $\Delta > 1$  (see Fig. 2(d)), the tagged-particle position admits the following form:

$$x_{s,i}(t) = (v_s^\sigma)^{\text{eff}} t + \sqrt{D_s} t^{1/2} H_{\Delta>1}(t) \xi_G + O(t^0 s^2), \quad (9)$$

with  $\xi_G$  a mean-zero, unit-variance normal (up to finite-time effects) random variable and  $D_{s \gg 1} = D_\infty$ . At the isotropic point  $\Delta = 1$ , by contrast, the crossover time scales as  $t_*(s) \sim s^3$ , such that, see Fig. 2(b):

$$x_{s,i}(t) \simeq (v_s^\sigma)^{\text{eff}} t + \sqrt{\kappa_G s t} H_{\Delta=1}(t/s^3) \xi_{G\text{-KPZ}}^\sigma + O(t^0 s), \quad (10)$$

where the unit-variance random variable  $\xi_{G\text{-KPZ}}^\sigma$  crosses over from a *skewed* (whose sign is given by  $\sigma$ ) random variable for  $t/s^3 \ll 1$  (see Fig. 2(a)), compatible with the Baik–Rains (BR) distribution characterizing stationary growing-interface fluctuations in the KPZ equation [114–117], to a normal Gaussian one for  $t/s^3 \gg 1$ . Namely, trajectory fluctuations around their mean exhibit a crossover from KPZ to normal dynamics, similarly (yet opposite in time) to crossovers between different statistics known for the KPZ equation and the WASEP model [118, 119].

The origin of such a crossover is manifested at the level of a single trajectory (see Fig. 1). For  $\Delta > 1$ , the bare velocities of large- $s$  particles are exponentially suppressed, and heavy rods are effectively immobile; their motion is dominated by frequent collisions with light species with random left/right chiralities, resulting in an incoherent random walk and rapid convergence to Eq. (9). At  $\Delta = 1$ , heavy quasiparticles retain a parametrically larger bare velocity and can undergo rare but substantial displacements through collisions with other large, mobile species. At short times, the dynamics of quasiparticles of species  $s$  are dominated by collisions with quasiparticles of species  $s' < s$ , where the dominant  $s'$  grows over time as more collisions occur. The associated scattering shift  $2s'$  is time-dependent, giving rise to anomalous transport. Eventually, at late times, the dominant scattering events involving species  $s$  are with species  $s' > s$ . The associated scattering shift  $2s$  is the maximum one possible for species  $s$ , so the dynamics in this regime is a random walk with a step size  $\sim 2s$ . Nevertheless, the heavy-tail statistics of these intermittent events yield the KPZ terms in Eq. (10).

**Charge transport.** We now move to the analysis of charge (spin) fluctuations. We focus on thermal equilibrium and study the statistics of the time variation of the total charge contained in the left half-system. We define the charge transfer as

$$\delta m(t) = \sum_{s \geq 1} \delta m_s(t), \quad \delta m_s(t) = \sum_{x < 0} s(N_s(x, t) - N_s(x, 0)), \quad (11)$$

with  $N_s(x, t) = \sum_i \delta(x - x_{s,i})$ . Previous works could only numerically access the full magnetization transfer. In our

model, we are able to directly resolve the magnetization transfer by species, and thus to explore how the contributions of different string species combine. In particular, we will find that *inter-species correlations* play an important part in fixing the asymptotics of the magnetization transfer.

First, we analyze the diffusion constant for the total spin  $\delta m$ . Using that the (time-averaged) charge (spin) diffusion constant  $\bar{\mathfrak{D}}_s(t)$  can be written in terms of the current  $J_m$  of  $m$  as  $\bar{\mathfrak{D}}(t) = \frac{d}{dt} \int_0^t dt' \int_0^t dt'' \langle J_m(t') J_m(t'') \rangle$ , and using Eq. (10), we arrive at (see End Matter for more details),

$$\bar{\mathfrak{D}}(t) \propto \int_0^t dt' \sum_{s \geq 1} \frac{\rho_s |(v_s^\sigma)^{\text{eff}}|^2 s^4}{\left| (v_s^\sigma)^{\text{eff}} t + \sqrt{\kappa_G s t} H_{\Delta=1}(t/s^3) \right|} \sim t^{1/3}, \quad (12)$$

giving the KPZ dynamical exponent  $z = 3/2$ , which was previously observed numerically and derived by kinetic-theory arguments [58, 108]. Remarkably, this result is *independent* of the precise scaling function  $H_{\Delta=1}(z)$  and, in particular, of the numerically observed KPZ scaling  $H(z) \simeq z^{-1/6}$  at small  $z$ : i.e. from the fact that the single trajectories themselves appear to obey KPZ scaling. The only relevant ingredient for the KPZ dynamical exponent being the crossover time  $t^* \sim s^3$ .

We remark that as quasiparticles move ballistically at the microscopic level, and all species carry positive charge, one might expect the fluctuations  $\delta m_s(t)$  to be ballistic. This is indeed true at asymptotically late times. However, at earlier times the corrections to ballistic transport in Eqs. (9), (10) are large: it is precisely these corrections that induce a crossover at a parametrically late time  $t_*(s) \sim s^{2z}$ , where  $z$  is the transport exponent (3/2 for  $\Delta = 1$ , 2 for  $\Delta > 1$ ), such that

$$\langle (\delta m_s(t))^2 \rangle \sim \begin{cases} t^{1/z}, & t \ll t_*(s), \\ v_s^{\text{eff}} t + O(t^{1/z}) & t \gg t_*(s), \end{cases} \quad (13)$$

This crossover is visible in Fig. 3, where the curves collapse when plotted as a function of  $t/t_*(s)$ .

The total magnetization fluctuations receive contributions from the variance of each species *and* from inter-species correlations,

$$\langle \delta m(t)^2 \rangle = \sum_{s \geq 1} \langle \delta m_s(t)^2 \rangle + \sum_{s \neq s'} \langle \delta m_s(t) \delta m_{s'}(t) \rangle. \quad (14)$$

Crucially, once a given species becomes ballistic, its diagonal contribution would, by itself, generate ballistic fluctuations of  $\delta m(t)$ . This does *not* happen because the off-diagonal terms in Eq. (14) conspire to cancel the ballistic contribution: ballistic species are effectively “screened out” of the total magnetization by the strong correlations between particles induced by the scattering shift in Eq. (2) (see End Matter for more details). This screening

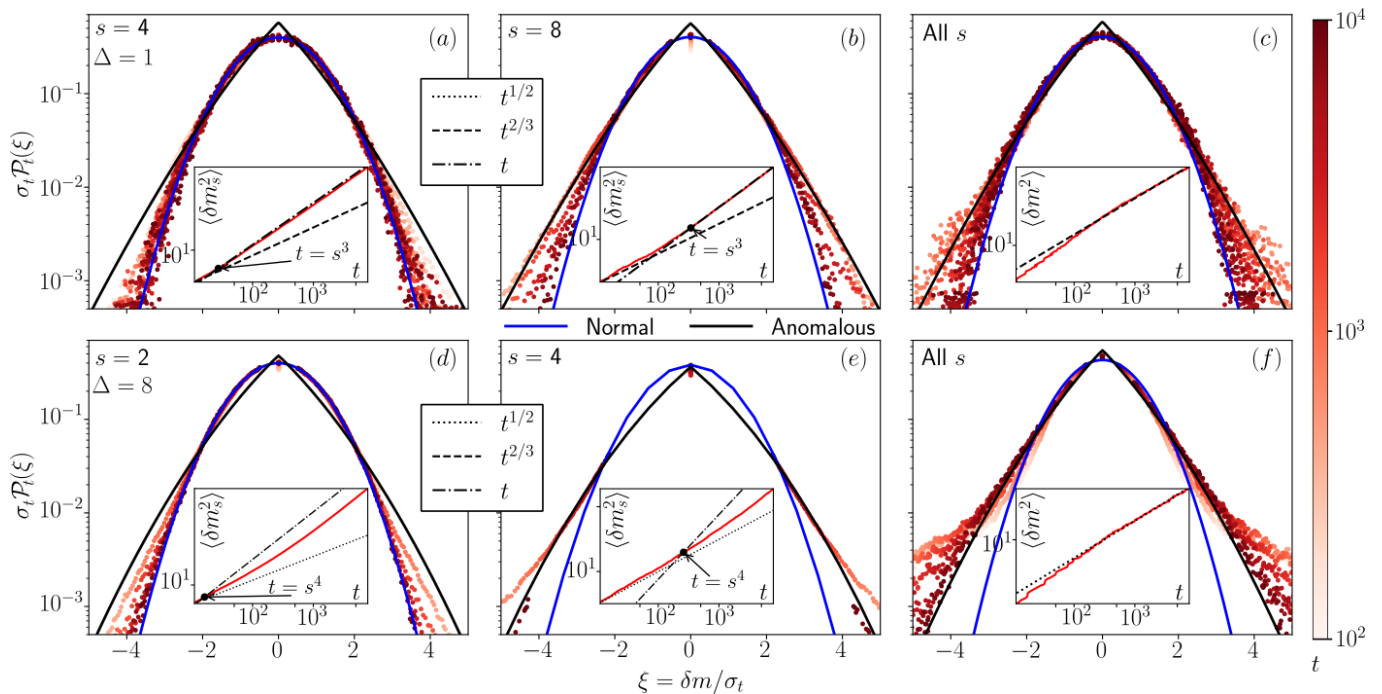


Figure 4. Plots of rescaled distributions of magnetic fluctuations for specific string species  $\mathcal{P}_t(\delta m_s)$  and the total magnetic fluctuations due to all particle species  $\mathcal{P}_t(\delta m)$ , see Eq. (11) (right-most column) for both  $\Delta = 1$  (top) and  $\Delta = 8$  (bottom). These are compared with both the anomalous non-Gaussian distribution of Eq. (17) (with  $\mathcal{P}_t$  the KPZ scaling function  $f_{\text{KPZ}}$  for  $\Delta = 1$  and the normal distribution for  $\Delta = 8$ ) and a normal distribution. All distributions are rescaled to have unit variance. The insets show the variance as a function of  $t$ .

mechanism has strong consequences not only for the scaling of cumulants, but also for the full counting statistics (FCS) of charge transfer, i.e. the full distribution  $P_t(\delta m)$ .

*Anisotropic regime:  $\Delta > 1$ .*— We first analyze the anisotropic case  $\Delta > 1$ . Here the largest particles with  $s \rightarrow \infty$  have exponentially small bare velocities and remain effectively immobile. As a consequence, even for  $t \gg t_*$  their contribution to  $\delta m(t)$  is not screened out. However, their charge fluctuations are not those of ordinary Brownian diffusion (as is the case for their trajectories; see Eq. (9)): their charge evolves according to a stochastic velocity  $v_\infty$  that fluctuates due to scatterings with the light particles. At the coarse-grained level, therefore, the magnetization density obeys an effective continuity equation

$$\partial_t m + \partial_x (v_\infty m) = 0. \quad (15)$$

In equilibrium  $\langle v_\infty \rangle = 0$ , but  $v_\infty$  exhibits non-trivial space-time fluctuations inherited from the initial (thermal) configurations. Solving Eq. (15) by characteristics for an initial profile  $m(x, 0) = m_0(x)$  gives  $m(x, t) = \int dx_0 m_0(x_0) \delta(x - x_\infty(x_0, t))$ , where the characteristic position of the large particle  $x_\infty(x_0, t)$  satisfies  $\partial_t x_\infty = v_\infty(x_\infty, t)$  with  $x_\infty(x_0, t = 0) = x_0$ . Since  $v_\infty$  is random with short-ranged temporal correlations at fixed  $x$ , the characteristic is expected to be diffusive, given by eq. (9) with  $s \rightarrow \infty$ . At long times, we may therefore evaluate

the advected fields on the mean (Euler) trajectory (here corresponding to zero drift velocity), effectively replacing  $v_\infty(x_\infty, \tau)$  by  $v_\infty(x, \tau)$ . This leads to the approximation

$$m(x, t) \approx m_0 \left( x - \int_0^t dt' v_\infty(x, t') \right). \quad (16)$$

This equation can be used to evaluate various quantities, including full counting statistics, which is given in terms of an anomalous, non-normal distribution [78–81, 83], expressed as a product of two random variables,

$$P_t(Q) = \int_{-\infty}^{\infty} dx_\infty \mathcal{P}_t(x_\infty) \frac{e^{-Q^2/(2\chi|x_\infty|)}}{\sqrt{2\pi\chi|x_\infty|}}, \quad (17)$$

one coming from the fluctuations of the initial state in terms of the magnetic susceptibility  $\chi$  (e.g.  $P(m_0) \sim e^{-(m_0)^2/(2\chi)}$ ), and  $\mathcal{P}_t(x_\infty)$  taken to be normal with zero mean and variance  $2D_\infty t$ , giving the fluctuations of  $v_\infty$ . This distribution describes both the fluctuations of  $\delta m_s$  with  $s \gg 1$  and of the total charge  $\delta m$ ; see Fig. 4 (e,f). Indeed, due to screening, the latter is given by  $\delta m \sim \sum_{s \sim t^{1/4}} \delta m_s$ , the sum of random variables that all fluctuate in the same way, and therefore the distribution remains the same (see also below).

Moreover, the *charge (spin) structure factor* can be related to the probability distribution of  $x_\infty(t) = \int_0^t dt' v_\infty(x, t')$ :  $C(x, t) = \langle m(x, t) m(0, 0) \rangle \propto \langle C_0(x -$

$x_\infty(t)$ ), where  $C_0(x)$  is the profile of the initial correlations. When the latter is a  $\delta(x)$  function, the structure factor is precisely the distribution of the fluctuations of the largest-particle trajectory, which is purely Gaussian. In this hard-rods model, however, equilibrium correlations have a non-trivial structure: convolving these with a Gaussian gives the correct result; see Fig. 5.

*Isotropic point:*  $\Delta = 1$ .— At the isotropic point there is no *maximal* quasiparticle  $s = \infty$ . Instead, for every string species  $s$ , the effective trajectory exhibits a crossover, at the screening time  $t_*(s) \sim s^3$ , from KPZ fluctuations to ballistic motion with diffusive broadening; see Eq. (10). For  $t \ll t_*(s)$ , the magnetization transfer  $\delta m_s$  follows the same probability distribution as in the gapped regime, see Fig. 4 (b), with  $x_\infty$  replaced by  $x_s$ . In particular, its distribution retains the anomalous form of eq. (17), but with  $\mathcal{P}_t(x_s)$  given by a symmetric law whose variance grows as  $\sim s t^{1/3}$ , in agreement with Eq. (10). In Fig. 4 (a,b,c) we chose to use the (expected) universal scaling function  $\mathcal{P}_t = f_{\text{KPZ}}$  even if numerically, and analytically, we are unable to determine its precise form. For  $t \gg t_*(s)$ ,  $\delta m_s$  crosses over to ballistic behavior and  $P(\delta m_s)$  crosses over to a normal distribution, as also observed in Fig. 4(b). A similar crossover from Eq. (17) to a normal distribution, albeit via a different mechanism, occurs at the level of the *total* magnetization fluctuations; see Fig. 4 (c). Due to screening, at time  $t$  only species with  $s \sim t^{1/3}$  contribute appreciably to  $\delta m$ , so that  $\delta m$  can be viewed as an effective sum over many species,

$$\delta m \sim \sum_{s \sim t^{1/3}} \delta m_s. \quad (18)$$

As  $t$  increases, this sum involves a growing number of (weakly) correlated random variables and, by the central limit mechanism, its distribution approaches a Gaussian. Crucially, the decorrelation between different contributions  $\delta m_{s=\bar{s}t^{1/3}}$  occurs algebraically, with correlations decaying as  $t^{-1/3}$  (see Fig. 6), in sharp contrast to the anisotropic regime where the relevant large- $s$  modes remain essentially identical and fully correlated. These results resolve the apparent tension reported in earlier works between KPZ scaling of dynamical correlations and the near-Gaussian shape of magnetization-fluctuation distributions at accessible numerical times.

**Conclusion.** We have introduced a hard-rods-like model with multiple species and only two velocities that captures the entire phase diagram of the spin dynamics of the XXZ chain. The model remarkably reproduces much of the transport physics of the quantum model and clarifies the origin of different physical phenomena, such as screening and the emergence of Gaussian correlations in the magnetization, that were previously only conjectured. Moreover, it reveals yet another manifestation of KPZ physics in these models, namely in the fluctuations of the trajectories of large quasiparticles. Several questions remain open. First, while here we could not derive

analytically the emergence of KPZ statistics for particle trajectories, we believe the model is sufficiently simple to enable future, more mathematical studies. Second, it is striking that KPZ scaling is found both in the dynamics of individual trajectories and in the net magnetization transport. The precise relation between these phenomena, however, remains to be understood. We expect that the model proposed here will serve as a simpler setting for such investigations, with possible analytical studies via ballistic MFT [83, 93, 120, 121], in the near future.

**Acknowledgments.** We thank Jitendra Kethepalli and Benjamin Doyon for discussions and collaborations on related topics. J.D.N., and A.U. are funded by the ERC Starting Grant 101042293 (HEPIQ) and the ANR-22-CPJ1-0021-01. This work was granted access to the HPC resources of IDRIS under the allocation AD010613967R2 and AD010613967R1.

- 
- [1] O. A. Castro-Alvaredo, B. Doyon, and T. Yoshimura, *Phys. Rev. X* **6**, 041065 (2016).
  - [2] B. Bertini, M. Collura, J. De Nardis, and M. Fagotti, *Phys. Rev. Lett.* **117**, 207201 (2016).
  - [3] M. Schemmer, I. Bouchoule, B. Doyon, and J. Dubail, *Phys. Rev. Lett.* **122**, 090601 (2019).
  - [4] B. Doyon, J. Dubail, R. Konik, and T. Yoshimura, *Phys. Rev. Lett.* **119**, 195301 (2017).
  - [5] J. De Nardis, D. Bernard, and B. Doyon, *Phys. Rev. Lett.* **121**, 160603 (2018).
  - [6] J. D. Nardis, D. Bernard, and B. Doyon, *SciPost Phys.* **6**, 49 (2019).
  - [7] B. Doyon, *SciPost Phys. Lect. Notes*, 18 (2020).
  - [8] B. Doyon and J. Durnin, *Journal of Statistical Mechanics: Theory and Experiment* **2021**, 043206 (2021).
  - [9] B. Doyon and H. Spohn, *SciPost Phys.* **3**, 039 (2017).
  - [10] B. Doyon, *J. Stat. Phys.* **186**, 25 (2022).
  - [11] J. Durnin, M. J. Bhaseen, and B. Doyon, *Phys. Rev. Lett.* **127**, 130601 (2021).
  - [12] B. Doyon, H. Spohn, and T. Yoshimura, *Nucl. Phys. B* **926**, 570 (2018).
  - [13] A. De Luca, J. Viti, L. Mazza, and D. Rossini, *Phys. Rev. B* **90**, 161101 (2014).
  - [14] A. Bastianello, B. Bertini, B. Doyon, and R. Vasseur, *J. Stat. Mech. Theory Exp.* **2022**, 014001 (2022).
  - [15] F. S. Møller, G. Perfetto, B. Doyon, and J. Schmiedmayer, *SciPost Phys. Core* **3**, 16 (2020).
  - [16] A. Bastianello, B. Doyon, G. Watts, and T. Yoshimura, *SciPost Phys.* **4**, 45 (2018).
  - [17] B. Bertini, F. Heidrich-Meisner, C. Karrasch, T. Prosen, R. Steinigeweg, and M. Žnidarič, *Rev. Mod. Phys.* **93**, 025003 (2021).
  - [18] A. Bastianello and A. De Luca, *Phys. Rev. Lett.* **122**, 240606 (2019).
  - [19] V. B. Bulchandani, S. Gopalakrishnan, and E. Iliievski, *J. Stat. Mech. Theory Exp.* **2021**, 084001 (2021).
  - [20] B. Doyon and F. Hübner, (2023), [arXiv:2307.09307](https://arxiv.org/abs/2307.09307).
  - [21] F. Møller, P. Schüttelkopf, J. Schmiedmayer, and S. Erne, *Phys. Rev. Res.* **6**, 013328 (2024).
  - [22] N. Malvania, Y. Zhang, Y. Le, J. Dubail, M. Rigol, and

- D. S. Weiss, *Science* **373**, 1129 (2021).
- [23] F. Møller, F. Cataldini, and J. Schmiedmayer, *SciPost Phys. Core* **7**, 025 (2024).
- [24] P. Ruggiero, P. Calabrese, B. Doyon, and J. Dubail, *Phys. Rev. Lett.* **124**, 140603 (2020).
- [25] F. Møller, N. Besse, I. E. Mazets, H.-P. Stimming, and N. J. Mauser, *Journal of Computational Physics* **493**, 112431 (2023).
- [26] V. B. Bulchandani, R. Vasseur, C. Karrasch, and J. E. Moore, *Phys. Rev. B* **97**, 045407 (2018).
- [27] F. Møller, S. Erne, N. J. Mauser, J. Schmiedmayer, and I. E. Mazets, (2022), [arXiv:2205.15871](https://arxiv.org/abs/2205.15871).
- [28] A. Bastianello, V. Alba, and J.-S. Caux, *Phys. Rev. Lett.* **123**, 130602 (2019).
- [29] F. Møller, B. C. Nagy, M. Kormos, and G. Takács, (2024), [arXiv:2411.11473](https://arxiv.org/abs/2411.11473).
- [30] I. Bouchoule, B. Doyon, and J. Dubail, *SciPost Phys.* **9**, 44 (2020).
- [31] B. Doyon, S. Gopalakrishnan, F. Møller, J. Schmiedmayer, and R. Vasseur, *Phys. Rev. X* **15**, 010501 (2025).
- [32] T. Bonnemain, B. Doyon, and G. El, *Journal of Physics A: Mathematical and Theoretical* **55**, 374004 (2022).
- [33] A. Bastianello, Ž. Krajnik, and E. Ilievski, *Phys. Rev. Lett.* **133**, 107102 (2024).
- [34] L. Dubois, G. Thémèze, F. Nogrette, J. Dubail, and I. Bouchoule, *Phys. Rev. Lett.* **133**, 113402 (2024).
- [35] F. Møller, C. Li, I. Mazets, H.-P. Stimming, T. Zhou, Z. Zhu, X. Chen, and J. Schmiedmayer, *Phys. Rev. Lett.* **126**, 090602 (2021).
- [36] W. Kao, K.-Y. Li, K.-Y. Lin, S. Gopalakrishnan, and B. L. Lev, *Science* **371**, 296–300 (2021).
- [37] Y. Le, Y. Zhang, S. Gopalakrishnan, M. Rigol, and D. S. Weiss, *Nature* **618**, 494–499 (2023).
- [38] F. Cataldini, F. Møller, M. Tajik, J. a. Sabino, S.-C. Ji, I. Mazets, T. Schweigler, B. Rauer, and J. Schmiedmayer, *Phys. Rev. X* **12**, 041032 (2022).
- [39] P. Schüttelkopf, M. Tajik, N. Bazhan, F. Cataldini, S.-C. Ji, J. Schmiedmayer, and F. Møller, (2024), [arXiv:2406.17569](https://arxiv.org/abs/2406.17569).
- [40] D. Wei, A. Rubio-Abadal, B. Ye, F. Machado, J. Kemp, K. Srakaew, S. Hollerith, J. Rui, S. Gopalakrishnan, N. Y. Yao, I. Bloch, and J. Zeiher, *Science* **376**, 716 (2022).
- [41] M. Horvath, A. Bastianello, S. Dhar, R. Koch, Y. Guo, J.-S. Caux, M. Landini, and H.-C. Nägerl, (2025), [arXiv:2505.10550](https://arxiv.org/abs/2505.10550).
- [42] L. Dubois, G. Thémèze, J. Dubail, and I. Bouchoule, (2025), [arXiv:2505.05839](https://arxiv.org/abs/2505.05839).
- [43] X. Zotos, F. Naef, and P. Prelovšek, *Phys. Rev. B* **55**, 11029 (1997).
- [44] X. Zotos, *Phys. Rev. Lett.* **82**, 1764 (1999).
- [45] T. Prosen, *Phys. Rev. Lett.* **106**, 217206 (2011).
- [46] T. Prosen, *Phys. Rev. Lett.* **111**, 057203 (2013).
- [47] E. Ilievski and J. De Nardis, *Phys. Rev. B* **96**, 081118 (2017).
- [48] A. Urichuk, Y. Oez, A. Klümper, and J. Sirker, *SciPost Phys.* **6**, 005 (2019).
- [49] A. Klümper and K. Sakai, *J. Phys. A: Math. Theor.* (2019), [arXiv:1904.11253](https://arxiv.org/abs/1904.11253).
- [50] C. Karrasch, J. H. Bardarson, and J. E. Moore, *Phys. Rev. B* **87**, 245128 (2013).
- [51] F. Heidrich-Meisner, A. Honecker, and W. Brenig, *Phys. Rev. B* **71**, 184415 (2005).
- [52] H. Spohn, *Journal of Statistical Physics* **154**, 1191 (2014).
- [53] M. Kulkarni, D. A. Huse, and H. Spohn, *Phys. Rev. A* **92**, 043612 (2015).
- [54] L. V. Delacrétaz and P. Glorioso, *Phys. Rev. Lett.* **124**, 236802 (2020).
- [55] S. Mukerjee, V. Oganesyan, and D. Huse, *Phys. Rev. B* **73**, 035113 (2006).
- [56] V. B. Bulchandani, S. Gopalakrishnan, and E. Ilievski, *Journal of Statistical Mechanics: Theory and Experiment* **2021**, 084001 (2021).
- [57] M. Ljubotina, M. Žnidarič, and T. Prosen, *Phys. Rev. Lett.* **122**, 210602 (2019).
- [58] S. Gopalakrishnan and R. Vasseur, *Phys. Rev. Lett.* **122**, 127202 (2019).
- [59] V. B. Bulchandani, *Phys. Rev. B* **101**, 041411 (2020).
- [60] J. De Nardis, S. Gopalakrishnan, E. Ilievski, and R. Vasseur, *Phys. Rev. Lett.* **125**, 070601 (2020).
- [61] E. Ilievski, J. De Nardis, S. Gopalakrishnan, R. Vasseur, and B. Ware, *Phys. Rev. X* **11**, 031023 (2021).
- [62] J. De Nardis, S. Gopalakrishnan, and R. Vasseur, *Phys. Rev. Lett.* **131**, 197102 (2023).
- [63] D. Wei, A. Rubio-Abadal, B. Ye, F. Machado, J. Kemp, K. Srakaew, S. Hollerith, J. Rui, S. Gopalakrishnan, N. Y. Yao, I. Bloch, and J. Zeiher, *Science* **10.1126/science.abk2397** (2022).
- [64] B. Ye, F. Machado, J. Kemp, R. B. Hutson, and N. Y. Yao, *Phys. Rev. Lett.* **129**, 230602 (2022).
- [65] K. A. Takeuchi, K. Takasan, O. Busani, P. L. Ferrari, R. Vasseur, and J. De Nardis, *Phys. Rev. Lett.* **134**, 097104 (2025).
- [66] M. Koterle, T. Prosen, and T. Zhou, (2026), [arXiv:2601.19894](https://arxiv.org/abs/2601.19894).
- [67] A. J. McRoberts, T. Bilitewski, M. Haque, and R. Moessner, *Phys. Rev. E* **106**, L062202 (2022).
- [68] A. J. McRoberts, T. Bilitewski, M. Haque, and R. Moessner, *Phys. Rev. B* **105**, L100403 (2022).
- [69] A. J. McRoberts and R. Moessner, *Phys. Rev. Lett.* **133**, 256301 (2024).
- [70] E. Tirrito, P. S. Tarabunga, D. S. Bhakuni, M. Dalmonte, P. Sierant, and X. Turkeshi, (2025), [arXiv:2506.12133](https://arxiv.org/abs/2506.12133).
- [71] C. Muzzi, D. S. Bhakuni, M. Dalmonte, L. Zadnik, and H. B. Xavier, (2025), [arXiv:2510.26897](https://arxiv.org/abs/2510.26897).
- [72] D. Wei, A. Rubio-Abadal, *et al.*, *Science* **10.1126/science.abk2397** (2022).
- [73] A. Scheie, N. E. Sherman, M. Dupont, S. E. Nagler, M. B. Stone, G. E. Granroth, J. E. Moore, and D. A. Tennant, *Nature Physics* **17**, 726 (2021).
- [74] E. Rosenberg, T. Andersen, *et al.*, *Science* **10.1126/science.adi7877** (2024).
- [75] K. A. Takeuchi, K. Takasan, O. Busani, P. L. Ferrari, R. Vasseur, and J. De Nardis, *Physical Review Letters* **134**, [10.1103/physrevlett.134.097104](https://arxiv.org/abs/10.1103/physrevlett.134.097104) (2025).
- [76] J. De Nardis, D. Bernard, and B. Doyon, *Phys. Rev. Lett.* **121**, 160603 (2018).
- [77] J. De Nardis, D. Bernard, and B. Doyon, *SciPost Phys.* **6**, 049 (2019).
- [78] S. Gopalakrishnan, D. A. Huse, V. Khemani, and R. Vasseur, *Phys. Rev. B* **98**, 220303 (2018).
- [79] Z. Krajnik, J. Schmidt, V. Pasquier, E. Ilievski, and T. Prosen, *Phys. Rev. Lett.* **128**, 160601 (2022).
- [80] Krajnik, Žiga and Ilievski, Enej and Prosen, Tomaž, *Phys. Rev. Lett.* **128**, 090604 (2022).
- [81] S. Gopalakrishnan, E. McCulloch, and R. Vasseur, *Proc.*

- Natl. Acad. Sci. U.S.A. **121**, [10.1073/pnas.2403327121](https://doi.org/10.1073/pnas.2403327121) (2024).
- [82] E. McCulloch, R. Vasseur, and S. Gopalakrishnan, *Phys. Rev. E* **111**, 015410 (2025).
- [83] T. Yoshimura and i. c. v. Krajenik, *Phys. Rev. E* **111**, 024141 (2025).
- [84] S. Gopalakrishnan and R. Vasseur, *Reports on Progress in Physics* **86**, 036502 (2023).
- [85] D. W. Jepsen, *Journal of Mathematical Physics* **6**, 405 (1965).
- [86] J. L. Lebowitz, J. K. Percus, and J. Sykes, *Phys. Rev.* **171**, 224 (1968).
- [87] J. Percus, *The Physics of Fluids* **12(8)**, 1560–1563 (1969).
- [88] C. Boldrighini, R. L. Dobrushin, and Y. M. Sukhov, *Journal of Statistical Physics* **31**, 577 (1983).
- [89] H. Spohn, *Large Scale Dynamics of Interacting Particles* (Springer-Verlag, Berlin, 1991).
- [90] C. Boldrighini and Y. M. Suhov, *Communications in Mathematical Physics* **189**, 577 (1997).
- [91] B. Pozsgay, T. Gombor, and A. Hutsalyuk, *Phys. Rev. E* **104**, 064124 (2021).
- [92] D. Bagchi, J. Kethepalli, V. B. Bulchandani, A. Dhar, D. A. Huse, M. Kulkarni, and A. Kundu, *Phys. Rev. E* **108**, 064130 (2023).
- [93] A. Kundu, (2025), [arXiv:2504.09201](https://arxiv.org/abs/2504.09201).
- [94] A. Urilyon, L. Biagetti, J. Kethepalli, and J. De Nardis, *Phys. Rev. B* **113**, 014314 (2026).
- [95] P. A. Ferrari and S. Olla, *The Annals of Applied Probability* **35**, [10.1214/24-aap2137](https://doi.org/10.1214/24-aap2137) (2025).
- [96] C. Moca, M. A. Werner, A. Valli, T. Prosen, and G. Zaránd, *Phys. Rev. B* **108**, 235139 (2023).
- [97] A. Valli, C. Moca, M. A. Werner, M. Kormos, i. c. v. Krajenik, T. c. v. Prosen, and G. Zaránd, *Phys. Rev. Lett.* **135**, 100401 (2025).
- [98] H. A. Bethe, *Zeitschrift für Physik* **71**, 205 (1931).
- [99] R. Orbach, *Physical Review* **112**, 309 (1958).
- [100] M. Takahashi, *Progress of Theoretical Physics* **46**, 401 (1971).
- [101] M. Takahashi, *Thermodynamics of One-Dimensional Solvable Models* (Cambridge University Press, Cambridge, 1999).
- [102] G. A. El, *Journal of Statistical Mechanics: Theory and Experiment* **2021**, 114001 (2021).
- [103] J. De Nardis, S. Gopalakrishnan, E. Ilievski, and R. Vasseur, *Phys. Rev. Lett.* **125**, 070601 (2020).
- [104] A. Klümper, *Zeitschrift für Physik B Condensed Matter* **91**, 507 (1993).
- [105] E. Ilievski, E. Quinn, J. De Nardis, and M. Brockmann, *Journal of Statistical Mechanics: Theory and Experiment* , 063101 (2016).
- [106] (2013), [arXiv:1302.2667](https://arxiv.org/abs/1302.2667) [cond-mat.str-el].
- [107] J. De Nardis, S. Gopalakrishnan, R. Vasseur, and B. Ware, *Proceedings of the National Academy of Sciences* **119**, [10.1073/pnas.2202823119](https://doi.org/10.1073/pnas.2202823119) (2022).
- [108] J. De Nardis, S. Gopalakrishnan, R. Vasseur, and B. Ware, *Phys. Rev. Lett.* **127**, 057201 (2021).
- [109] B. Doyon, J. Durnin, and T. Yoshimura, *SciPost Phys.* **13**, 072 (2022).
- [110] T. Bonnemain, V. Caudrelier, and B. Doyon, *Annales Henri Poincaré* [10.1007/s00023-025-01546-2](https://doi.org/10.1007/s00023-025-01546-2) (2025).
- [111] A. Aggarwal, (2025), [arXiv:2503.08018](https://arxiv.org/abs/2503.08018).
- [112] B. Doyon, F. Hübner, and T. Yoshimura, *Phys. Rev. Lett.* **132**, 251602 (2024).
- [113] B. Doyon and H. Spohn, *Journal of Statistical Mechanics: Theory and Experiment* **2017**, 073210 (2017).
- [114] M. Kardar, G. Parisi, and Y.-C. Zhang, *Physical Review Letters* **56**, 889 (1986).
- [115] C. A. Tracy and H. Widom, *Communications in Mathematical Physics* **159**, 151 (1994).
- [116] M. Prähofer and H. Spohn, *Journal of Statistical Physics* **108**, 1071 (2002).
- [117] I. Corwin, *Random Matrices: Theory and Applications* **1**, 1130001 (2012).
- [118] T. Sasamoto and H. Spohn, *Journal of Statistical Physics* **140**, 209–231 (2010).
- [119] P. Le Doussal, *Journal of Statistical Mechanics: Theory and Experiment* **2017**, 053210 (2017).
- [120] B. Doyon, G. Perfetto, T. Sasamoto, and T. Yoshimura, *SciPost Phys.* **15**, 136 (2023).
- [121] J. Kethepalli, A. Urilyon, T. Sadhu, and J. D. Nardis, (2025), [arXiv:2505.18093](https://arxiv.org/abs/2505.18093).

## End Matter

Supplemental numerical data.

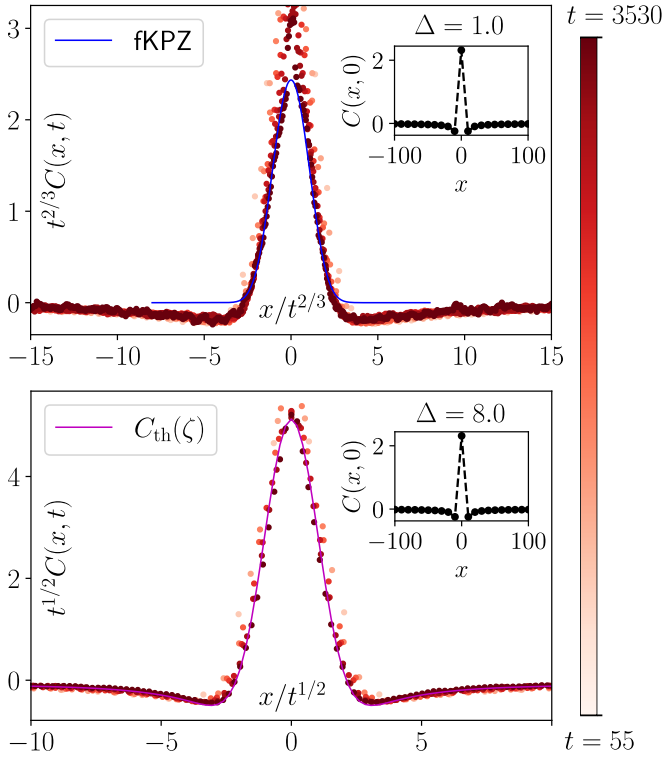


Figure 5. Rescaled correlation function  $C(x, t) = \langle m(x, t)m(0, 0) \rangle_c$  for both  $\Delta = 8$  and  $\Delta = 1$ . In either anisotropy, the scaling is significantly different between the anisotropies. For  $\Delta = 8$  the evolution is well described by convolving the initial correlation with the diffusion kernel (continuous line). For  $\Delta = 1$  the correct convolution is not known, and we show the disagreement with the (naive) distribution  $f_{\text{KPZ}}$ . The insets show the value of the equilibrium correlation at  $t = 0$  showing that it is not a  $\delta(x)$  function.

**Vanishing ballistic part of magnetisation.** In the large anisotropy limit there are two distinct spin types, the ballistic particles  $s = 1$ , and the immobile particles  $s > 1$ . The magnetization fluctuation is noted as being closely associated with the number fluctuation

$$\delta m_s = s(N_s^L - N_s^R) = s \delta N_s, \quad (19)$$

where  $\rho_s = \frac{1}{s(s+1)(s+2)}$ . The number fluctuation of an immobile string is proportional to  $-\delta N_1$ , since an excess of right moving  $s = 1$  particles induces a leftward motion of the immobile string. This proportionality can be fixed by noting that any immobile string - magnon collision leads to a shift of  $\alpha_{1,s} = 2$ , whereas magnon-magnon collisions lead to shifts  $\alpha_{1,1} = 1$ . This shift can be combined with the likelihood of a ballistic - immobile string collision ( $\langle N_s^{\text{coll}} \rangle = tv_1 \rho_s$ ) to imply that the ballistic fluctuations for the immobile particles are given by

$$\frac{\delta N_1}{\rho_1} = -\frac{2\delta N_s}{\rho_s}. \quad (20)$$

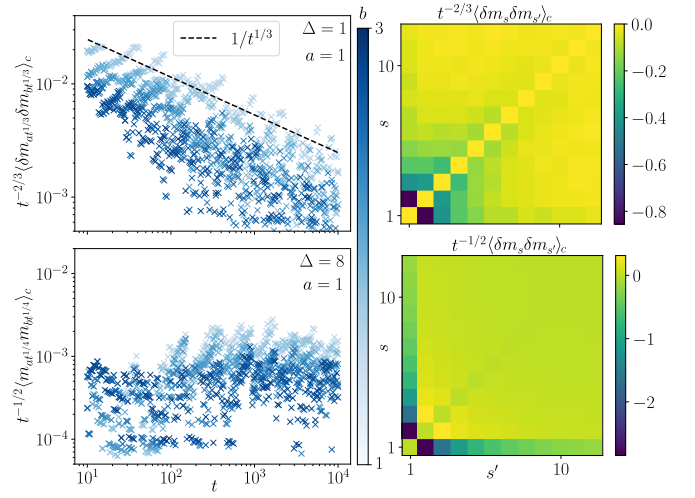


Figure 6. The evolution of the off-diagonal part of the correlation function. In the left plot, the off-diagonal correlation function, divided by the diagonal strength, is plotted with rescaled spins  $s = at^{1/2z}$  and  $s' = bt^{1/2z}$ , where  $a = 1$  and  $b$  is changed, with darker blue implying larger  $b$ . The rescaled correlation function is observed to decay in time as  $t^{-1/3}$  when  $\Delta = 1$ , implying the validity of the CLT, whereas for  $\Delta = 8$  the rescaled correlation function is constant, suggesting the failure of the CLT. In the second column, the time-scaled off-diagonal part of the correlation functions is plotted at  $t \sim 8000$ . From these plots the  $\Delta = 8$  correlation is found to be dominated by the magnon-string interactions, and it is uniformly non-zero at large particles, while for  $\Delta = 1$  it vanishes for large particles.

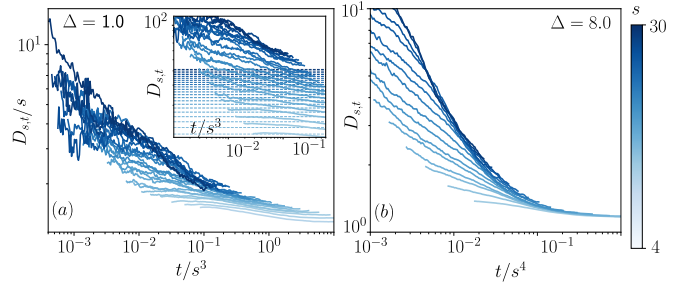


Figure 7. Plot of finite-time diffusion constant  $D_{s,t} = \langle (\delta x_s(t) - \langle \delta x_s \rangle)^2 \rangle / t$  against rescaled time for each particle species. In plot (a) the diffusion constant is rescaled by the string length with the expectation that  $D_{s,t}/s \xrightarrow{s \rightarrow \infty} \text{const}$  and the result demonstrated the collapse of large particles to a single curve, the inset shows the unscaled values and dashed lines indicating the asymptotic diffusion, see Eq. (42). In plot (b) all particles are found to approach the same diffusion constant as expected.

These ballistic-scale identities are inserted into the total magnetization fluctuation, which after some algebra is rewritten as

$$\langle \delta m^2 \rangle = \langle \delta m_1^2 \rangle \left( 1 - \sum_{s>1} s \frac{\rho_s}{2\rho_1} \right)^2 + O(\sqrt{t}) \quad (21)$$

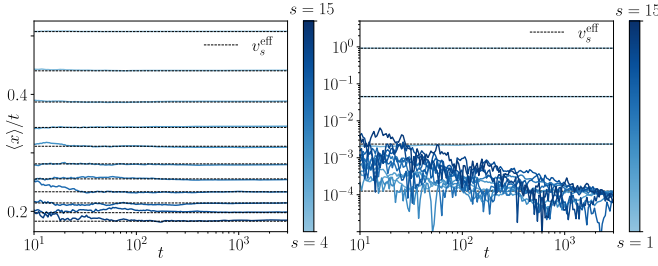


Figure 8. The analytical value of  $v_s^{\text{eff}}$  (defined in Eq. (6)) is plotted as a dotted line over the numerically determined velocity for each string type, evaluated as  $\langle x_{s,i}(t) \rangle / t$  where  $x_{s,i} = x_{s,i}(t) - x_{s,i}(0)$  for  $\Delta = 1$  (left) and  $\Delta = 8$  (right).

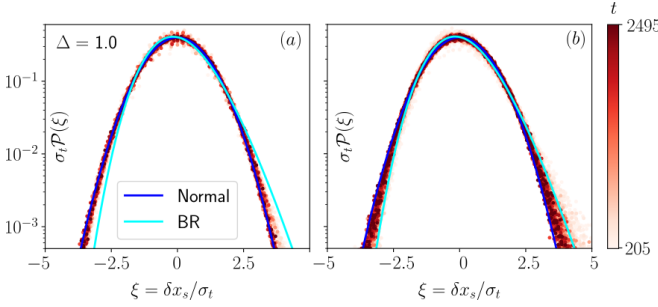


Figure 9. Plot of the distribution of fluctuations  $\mathcal{P}(\delta x_s)$  (also averaged with left movers  $\xi \rightarrow -\xi$ ) for  $\Delta = 1$ . The left panel, plot (a), shows the smallest strings,  $s = 1 - 5$ , whose fluctuations are consistent with a Gaussian distribution. In the right panel, plot (b), intermediate sized strings,  $s = 6 - 10$ , are plotted and demonstrate a transition from a Baiks-Rains distribution to a Gaussian distribution. These distributions are rescaled to have unit variance and zero mean.

The evaluation of the sum in the brackets,  $\sum_{s>1} s \frac{\rho_s}{2\rho_1} = \sum_{s>1} \frac{3}{(s+1)(s+2)} = 1$ , exactly cancels the bracketed term and leaves only the  $O(\sqrt{t})$  terms, thereby ensuring that the magnetization is not ballistic. It is worth pointing out is that this cancellation relies on the form of the density and implies that away from half filling ballistic growth of the magnetization variation can occur.

**Derivation of the spin diffusion constant.** Starting from eq. 16, we find that the spin diffusion constant is given by the variance  $\langle x_\infty^2 \rangle = 2\mathfrak{D}t + \dots$  of the quantity  $x_\infty(t) = \int_0^t dt v_\infty(0, t)$ . The average  $\langle v_\infty(x, t) \rangle = 0$  vanishes for  $\Delta \geq 1$ , but there are non-trivial space-time fluctuations due to thermal fluctuations in the initial state. Within linear response, note that

$$\delta v_\infty = \sum_{s,\sigma} \frac{\delta v_\infty}{\delta n_{s,\sigma}} \delta n_{s,\sigma} + \dots \quad (22)$$

where the functional derivative is evaluated in the background equilibrium state, whereas the fluctuations  $\delta n_{s,\sigma}(x, t)$  are simply advected from the initial state along the particle trajectories. We then define a time-

dependent diffusion constant from  $\mathfrak{D}(t) = \frac{1}{2} \frac{d}{dt} \langle x_\infty^2(t) \rangle$ , so that

$$\mathfrak{D}(t) = \frac{1}{2} \frac{d}{dt} \lim_{s_0 \rightarrow \infty} \int_0^t dt' \int_0^t dt'' \sum_{s,s'} \sum_{\sigma,\sigma'} \frac{\delta v_{s_0}}{\delta n_{s,\sigma}} \frac{\delta v_{s_0}}{\delta n_{s',\sigma'}} \langle \delta n_{s,\sigma}(x_s(t)) \delta n_{s',\sigma'}(x_{s'}(t)) \rangle, \quad (23)$$

with the convective particle trajectories following eq. (10). Using the thermal fluctuations in the initial state

$$\langle \delta n_{s,\sigma}(x) \delta n_{s',\sigma'}(x') \rangle = \frac{\rho_s}{(\rho_s^{\text{tot}})^2} \delta_{s,s'} \delta(x - x') \delta_{\sigma,\sigma'}, \quad (24)$$

and using that

$$\lim_{s_0 \rightarrow \infty} \left( \frac{\delta v_{s_0}}{\delta n_{s,\sigma}} \right)^2 \propto s^4 ((v_s^\sigma)^{\text{eff}} \rho_s^{\text{tot}})^2, \quad (25)$$

we find (12) in the main text.

**Equivalence to hard rod contraction.** A better intuition for the role of the trajectories can be gained by restricting ourselves to a single particle species. In this case, the scattering kernel

$$\mathfrak{a}_{s,s'} = 2 \min(s, s') - \delta_{s,s'} \xrightarrow{s=1} 1 = \mathfrak{a}. \quad (26)$$

With this identification the bare coordinates, characterized by free point particles, for our multi-species model yields exactly the hard rod model by fixing  $s = 1$  thus reproducing hard-rods with length  $\mathfrak{a} = 1$ . Since there is only a single particle species it follows that

$$\begin{aligned} X_{s,i}^{(t)} &= x_{s,i}(t) + \frac{1}{2} \sum_{s',j} \mathfrak{a}_{s,s'} \text{sign}(x_{s,i}(t) - x_{s',j}(t)) \\ X_i^{(t)} &= x_i(t) + \frac{\mathfrak{a}}{2} \sum_j \text{sign}(x_i(t) - x_j(t)). \end{aligned} \quad (27)$$

This last line is exactly the contraction map for hard-rods [89].

**Details on the numerical procedure.** The broad sketch of the numerics used to generate the data in this paper follow the algorithm

- Prepare an initial state of bare particles
- Invert the contraction map, Eq. 4, and truncate the initial state of bare particles in interacting coordinates. Save the truncated bare particle coordinates, which now constitute the initial fluctuating state.
- Evolve this initial state forward in time (in bare coordinates) and invert the contraction map to determine  $x_{s,i}(t)$  saving these values as trajectories.

Each step must be done carefully and are elucidated below.

*Inverting the contraction map.*— Key to the wave packet gas method is to take the bare coordinates  $X_{s,i}$

and determine the corresponding interaction coordinates  $x_{s,i}$  of course inverting

$$X_{s,i}^{(t)} = x_{s,i}(t) + \frac{1}{2} \sum_{s',j} \mathbf{a}_{s,s'} \text{sign}(x_{s,i}(t) - x_{s',j}(t)) \quad (28)$$

directly is not particularly feasible, except in the case of only one particle species. Instead, consider a surface fixed by the bare coordinates with dependence on a continuous set of coordinates  $\tilde{x}$  and whose form is defined so that the minima yields the contraction map

$$S(\tilde{x}) := \sum_{s,i} \frac{(X_{s,i} - \tilde{x}_{s,i})^2}{2} + \sum_{(s,i),(s',j')} \mathbf{a}_{s,s'} \frac{|\tilde{x}_{s,i} - \tilde{x}_{s',j'}|}{4}. \quad (29)$$

By finding the solutions  $(x_1 \dots x_N)(t) = \text{Argmin}(S_{X,t}(\tilde{x}))$  for this (convex) surface the contraction map is thus inverted.

To aid in numerical minimization, the absolute value and sign functions are regularized with an arbitrary factor  $\alpha$  as

$$|x| \stackrel{\alpha \gg 1}{\approx} \frac{\log[(1 + e^{\alpha x})(1 + e^{-\alpha x})]}{\alpha}, \quad (30)$$

$$\text{sign}(x) \stackrel{\alpha \gg 1}{\approx} \tanh(\alpha x/2). \quad (31)$$

For the data used in the plots the minimization was done via L-BFGS-B algorithm. For increased precision, the regularization parameter  $\alpha$  is increased in steps, with the surface minimization results for small- $\alpha$  providing an initial input for larger- $\alpha$ . By gently increasing the regularization parameter the stability of the minimization scheme was found to be greatly improved.

*Bare particle initialisation.*— A target coarse grained interacting density,  $\bar{\rho}_s$ , is identified along with a corresponding coarse grained free density  $\bar{\rho}_s^F = \bar{\rho}_s/(1^{\text{dr}})$ , where  $1_s^{\text{dr}} = 1 - \sum_{s'} \mathbf{a}_{s,s'} \bar{\rho}_{s'}$  is a dependent factor that relates the bare to interacting coordinates and indicates the ‘allowed length’ through which the interacting particles propagate with their bare velocities. Each specie is distributed according to a Poisson point process, where the distance  $r_{s,i}$  between the nearest particles of the same type are sampled from a normalized exponential distribution  $P(r_s) = \rho_s^F e^{-\bar{\rho}_s^F r}$  along an axis of length  $L$ . Repeat this for each particle type  $s$ . Once placed, a particle is assigned a rapidity (or momenta), in our model simply  $\pm 1$ , however, more general assignments can also be made.

*Truncate the initial state.*— The contraction map is inverted for the combined (multi-species  $s = 1, 2 \dots$ ) coordinates to determine the interacting coordinates  $x_{s,i}$ . A truncation is made on the newly obtained interacting coordinates so that they all fall within a region  $x_{s,i} \in (-L/2, L/2)$ , and save the, now truncated, set of bare coordinates  $X_{s,i}$ .

*Time evolution.*— The system is now straightforwardly evolved, in the bare coordinates the particles have a velocity given by  $v_s$  with the time evolution

$$X_{s,i}^{(t)} = v_s t + X_{s,i}^{(0)} \quad (32)$$

the time value is arbitrary and the corresponding  $x_{s,i}(t)$  is determined by inverting the contraction map.

To reach longer times reflective boundary conditions can be introduced. This must be implemented in the bare coordinates to correctly account for reflection, so the reflective boundary will have different bare coordinate positions for difference particles specie

$$\pm \frac{L_s^{\text{ref}}}{2} = \pm \frac{L}{2} \pm \frac{1}{2} \sum_{s',j} \mathbf{a}_{s,s'}. \quad (33)$$

The time evolved bare coordinates are reflected back into the box as

$$X_{s,i}^{(r)}(t) = \frac{L_s^{\text{ref}}}{2} - |\text{mod}_{2L_s^{\text{ref}}}[X(t)] - L_s^{\text{ref}}|. \quad (34)$$

This is combined with a reflection number that counts for the number of reflections and combined with the above determines the total displacement of a particle.

#### *Exact solutions of thermodynamic functions.*

The simple form of the particle-particle scattering kernel in our model allows for the explicit computation of many relevant transport quantities. Key here is the notion of dressing, in which the single particle variable is modified by surrounding particles into an effective form. To determining the effective velocity a particle’s spatial displacement must be rescaled by the portion of space that supports particle presence, a so called allowed length, this factor is denoted here as  $1^{\text{dr}}$ . This allowed length factor is computed by summing all particles to remove the forbidden regions as

$$1_s^{\text{dr}} = 1 - \sum_s \mathbf{a}_{s,s'} \bar{\rho}_{s'} \quad (35)$$

with  $\bar{\rho} = 1/(s(s+1)(s+2))$  being the coarse grained particle density also introduced in the text. After inserting the scattering kernel  $\mathbf{a}_{s,s'} = 2\min(s, s') - \delta_{s,s'}$  the sum evaluates to

$$1_s^{\text{dr}} = 1 - \left( \frac{s^2 + s - 1}{s(2+s)} \right) = \frac{s+1}{s(s+2)}. \quad (36)$$

In our model, the effective velocity is found by rescaling the particle displacement by the allowed length

$$(v_s^\sigma)^{\text{eff}} = \lim_{t \rightarrow \infty} \frac{1}{1_s^{\text{dr}} t} \langle v_s^\sigma t \rangle = \frac{s(s+1)}{s+2} v_s^\sigma \quad (37)$$

yielding the form used in the text.

*General approach for dressing calculations.*— Generically, other variables can be understood as being 'dressed' by the identity

$$\sum_{s'} (\delta_{s,s'} + \mathbf{a}_{s,s'} n_{s'}) f_{s'}^{\text{dr}} = f_s, \quad (38)$$

where the new variable  $n_s = \bar{\rho}_s / 1_s^{\text{dr}} = 1/(s+1)^2$  is obtained by comparison with our calculation for the allowed length. The goal now is to rewrite this expression in a recursive form. The first step is to insert the scattering kernel and grouping terms

$$\begin{aligned} f_s &= (1 - n_s) f_s^{\text{dr}} + 2 \sum_{s'=1}^s s' n_{s'} f_{s'}^{\text{dr}} + 2s \sum_{s'=s+1} n_{s'} f_{s'}^{\text{dr}} \\ f_s^{\text{dr}} &= \frac{f_s - 2F_s}{1 - n_s}. \end{aligned} \quad (39)$$

By straightforward substitution a recursive formula for  $F_s$  is obtained

$$\begin{aligned} F_s &= \sum_{s'=1}^{s-1} (s' - s) n_{s'} f_{s'}^{\text{dr}} + s \sum_{s'=1} n_{s'} f_{s'}^{\text{dr}} \\ &= \sum_{s'=1}^{s-1} (s' - s) n_{s'} \frac{(f_{s'} - 2F_{s'})}{1 - n_{s'}} + s \sum_{s'=1} \rho_{s'} f_{s'} \end{aligned} \quad (40)$$

Now, given a function  $f_s$ , this recursive formula is used

to compute the function  $F_s$ , from which an ansatz is constructed and checked against a difference equation for  $F_s$  (following from the above equation). Thus determining the function  $F_s$  and fixing the form of the dressed function.

More concretely, the diffusive contribution from each particle relies on the dressed form of the scattering kernel. This must be treated with a simple modification  $F_s \rightarrow F_{s,s'}$ , with the note that the bare function is  $f_s \rightarrow \mathbf{a}_{s,s'}$ . With an additional note that the kernel satisfies the transpose identity  $\mathbf{a}_{s,s'}^{\text{dr}} = \mathbf{a}_{s',s}^{\text{dr}}$  and with the above method the explicit form of the dressed scattering kernel is found to be

$$\alpha_{s,s'}^{\text{dr}} = \frac{(\max(s, s') + 1)(\min(s, s') + 1)^2}{3 \max(s, s')(\max(\frac{s}{2}, \frac{s'}{2}) + 1)} - \delta_{s,s'} \frac{(1+s)^2}{s(2+s)}. \quad (41)$$

Note that this expression for the dressed scattering kernel allows us to directly calculate any dressed variable.

*Diffusion formula.*— With the analytical form of the dressed kernel and the effective velocity, the diffusion constant can also be determined. We separate the positive and negative components of the effective velocity, writing  $v_s^{\text{eff}} = 1/(s^2 1_s^{\text{dr}})$ , and note the convenient identity  $v_s^{\text{eff}} > v_{s'}^{\text{eff}}$  when  $s < s'$ . With this additional simplification, the diffusion constant for due to a single particle species

$$\begin{aligned} D_s &= \frac{2}{(1_s^{\text{dr}})^2} \left( v_s^{\text{eff}} \sum_{s'=s+1}^{\infty} \bar{\rho}_{s'} (\mathbf{a}_{s,s'}^{\text{dr}})^2 + \sum_{s'=1}^{s-1} v_{s'}^{\text{eff}} \bar{\rho}_{s'} (\mathbf{a}_{s,s'}^{\text{dr}})^2 + v_s^{\text{eff}} \bar{\rho}_s (\mathbf{a}_{s,s}^{\text{dr}})^2 \right) \\ &= \frac{8}{9} \sum_{s'=1}^{\infty} \min \left[ 1, \frac{(s+2)^3 s(s+1)}{(s'+2)^3 s'(s'+1)} \right] \left( \frac{s'+1}{s'} \right)^2 - \frac{2(1+4s)}{3s^2} \stackrel{s \rightarrow \infty}{\sim} \frac{10s}{9} \end{aligned} \quad (42)$$

An explicit summation is possible, although the closed form has an unwieldy form

$$\begin{aligned} D_s &= \left( P(s) - \frac{s(s+1)(s+2)^3}{9} \psi^{(2)}(s+1) + \frac{8}{9} \left( 2H_{s-1} + H_{s-1}^{(2)} \right) \right) \\ P(s) &:= \frac{2}{9s^2(s+1)^2} - \frac{s(s(s(2s(s+8)+29)+25)+28)+28}{18s(s+1)^2} \end{aligned} \quad (43)$$

with polygamma functions,  $\Psi^{(n)}(z) = \partial_z^{n+1} \ln \Gamma(z)$ , and generalized harmonic numbers  $H_{s-1}^{(n)} = \sum_{k=1}^{s-1} 1/k^n$